

Models to Predict the Magnetic Properties of Single- and Multiple-Bridged
Phosphate Cu^{II} Systems: A Theoretical DFT Insight.

Karina Muñoz-Becerra¹, Daniel Aravena^{1,2}, Verónica Paredes-García³, Eliseo Ruiz⁴,
Evgenia Spodine^{5,2}, Diego Venegas-Yazigi^{1,2*}

¹ Facultad de Química y Biología, Universidad de Santiago de Chile, USACH, Santiago, Chile.

² Centro para el Desarrollo de la Nanociencia y Nanotecnología, CEDENNA, Santiago, Chile.

³ Universidad Andres Bello, Departamento de Ciencias Químicas, Santiago, Chile.

⁴ Departament de Química Inorgànica and Institut de Química Teòrica i Computacional, Universitat de Barcelona, Barcelona, Spain.

⁵ Facultad de Ciencias Químicas y Farmacéuticas, Universidad de Chile, Santiago, Chile.

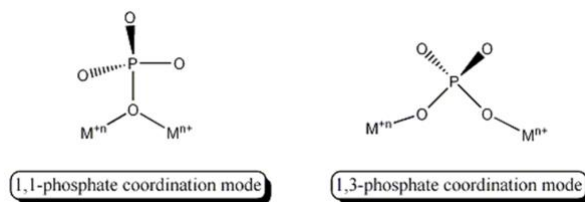
Corresponding author: diego.venegas@usach.cl

Abstract

Copper(II) phosphate bridged compounds have been studied by DFT methods in order to have a better understanding of the magnetic exchange interactions that are propagated by these 1,1 and 1,3- bridges, which varies due to the plasticity of the bonding modes of the ligand. An overview of related structures from the Cambridge Structural Database, CSD, shows that phosphate is generally bridging together with other ligands thus making difficult to assign the predominant exchange pathway. This work provides a graphical analysis, based on the unrestricted corresponding orbitals (UCO), which permits to obtain “magnetic”-like orbitals allowing a graphical assignment of the predominant exchange pathway. Models for the 1,1- and 1,3- bridging modes were developed in order to generate the angle dependence of J values. Thus, for the 1,1- bridging mode the Cu-O-Cu angle, θ , was used, while for the 1,3-phosphate a more sophisticated model including dummy atoms (D) was generated, defining the D-P-O_i-Cu_i dihedral angle (ϕ) for this bridging mode. Using models with different D-P-O_i-Cu_i dihedral angles a predictive scheme was generated. Eleven copper(II) phosphate bridged structures chosen from the CSD, were used to validate the proposed model. The study has shown that antiferromagnetic exchange interactions are primarily produced by phosphate bridges due to the plasticity of the bonding modes of the ligand that always enable a degree of overlap between the magnetic orbitals.

1. Introduction

Phosphate is a widely used ligand in inorganic and hybrid organic-inorganic materials, where it binds the metal centers with different coordination modes, that in a simple way can be classified as 1,1- and the classical 1,3- coordination modes (Scheme 1).



Scheme 1.

The great plasticity offered by the phosphate ion has permitted to identify from a structural point of view different notations to describe the coordination modes. For example, the work reported by Su et al. uses the Harris notation and shows systems in which one phosphate ion can be coordinated up to six metal ions at the same time. ¹ Hence, this ligand can be found in both molecular and extended polynuclear systems, where it is bridging two or more cationic centers. ²⁻¹⁵ As can be obtained from the Cambridge Structural Database, CSD¹⁶, many first transition metal ion phosphates have been reported, but copper based systems are one of the most studied. Among the molecular complexes, the best known are the dinuclear copper phosphate bridged ones, while the tetranuclear and trinuclear species have been less investigated. ^{9,15,17,18} Thus, the different magnetic patterns, ranging from almost isolated molecular dinuclear copper complexes to extended 3D frameworks, have generated several analyses with the use of both experimental and theoretical data. Several authors report that the 1,3-PO₄ coordination mode should produce a weaker magnetic coupling than the 1,1-PO₄ mode, where the interaction is through only one oxygen atom. ^{17,19-21}

The work published by Crawford et al. in 1976 is considered as one of the first attempts to correlate magnetic properties transmitted through one oxygen atom, with structural parameters. This work deals with planar di-hydroxido di-copper complexes with nitrogen containing ligands in the first coordination sphere. ²² These authors correlated the magnitude of the exchange parameter, J , with the value of the angle Cu-O-Cu of the

hydroxido complexes. Lately Ruiz et al., using DFT calculations, expanded the above-mentioned correlation by incorporating the out of plane displacement angle of the hydrogen atom of the hydroxido group.²³

Doyle et al. reported an experimental and theoretical study of a ferromagnetic tetranuclear copper(II) complex, where phosphate is the magnetic pathway. Both the 1,3- and 1,1-phosphate coordination modes are present in the studied complex. These authors point out the similarity that is observed for the hydroxido and the 1,1-phosphate bridging modes, as in both systems only one oxygen atom is involved in the exchange phenomenon.¹⁵ Another one oxygen atom magnetic exchange pathway can be mentioned, and this corresponds to the phenoxido group. Venegas-Yazigi et al. did a full analysis in 2010 using DFT calculations, of the different structural parameters of dinuclear copper species that influence the exchange through a phenoxido oxygen atom.²⁴

In the late seventies Lambert et al. proposed that the tetrahedrally oriented oxoanions showing pure sp^3 hybridization, such as ClO_4^- , PO_4^{3-} , and CrO_4^{2-} , should propagate ferromagnetic exchange interactions between copper ions.¹⁴ More recently Doyle et al. analyzed an arsenate bridged copper compound based on Lambert's statements. The resulting weak antiferromagnetic-coupled system was explained by the authors giving as one possible reason, the deviation of the bridgehead O-As-O angles from the perfect tetrahedral 109.5° value.²⁵ Moreover, several examples of 1,3-phosphate bridged copper compounds have been shown to be antiferromagnetically coupled.^{20,21} Therefore, more work is needed in order to contribute to the understanding of the magnitude and sign of the magnetic exchange interactions mediated by phosphate bridges, since it becomes evident that the exact mode of coordination of the phosphate group that determines the bridging mode and the bridging angles, and hence the exact orbitals involved in the transmission of the exchange phenomenon will affect the sign and magnitude of the coupling constant, J . If a search of P-O-Cu angles is performed in the CSD₁₆, 80 hits ranging from 112° to 162° are obtained. This result is showing that the oxygen from the phosphate group that acts as a bridge is always adopting a distorted tetrahedral geometry, i.e. the angles are larger than 109.5° . In the present work, we have generated structural models with the 1,1- and 1,3- PO_4 coordination modes and using DFT calculations the exchange parameter as a function of different structural distortions were evaluated. As discussed above, one phosphate bridge is

generally present together with other phosphate bridges or different auxiliary ligands generating a multiple bridged interaction.

In order to establish an intuitive link between the structural dependence of J and the magnetic orbital model of the exchange interaction, we have developed a graphical analysis based on the unrestricted corresponding orbitals (UCO).^{26,27} This representation allows the derivation of “magnetic”-like orbitals, as it reinforces one to one pairing of alpha and beta electrons to described doubly occupied orbitals. In this way, unpaired electrons are described by alpha orbitals that do not have a beta counterpart, being effectively “unpaired”. Magnetic orbitals derived in this way have proven to follow the Kahn-Briat model for systems with more than one unpaired electron per metal center.²⁸

2. Computational Details

All calculations were performed using the ORCA 3.0.3 program package.^{29,30} Molecular geometries for experimental complexes were obtained from the CSD database. The studied systems are detailed in Figure 1.

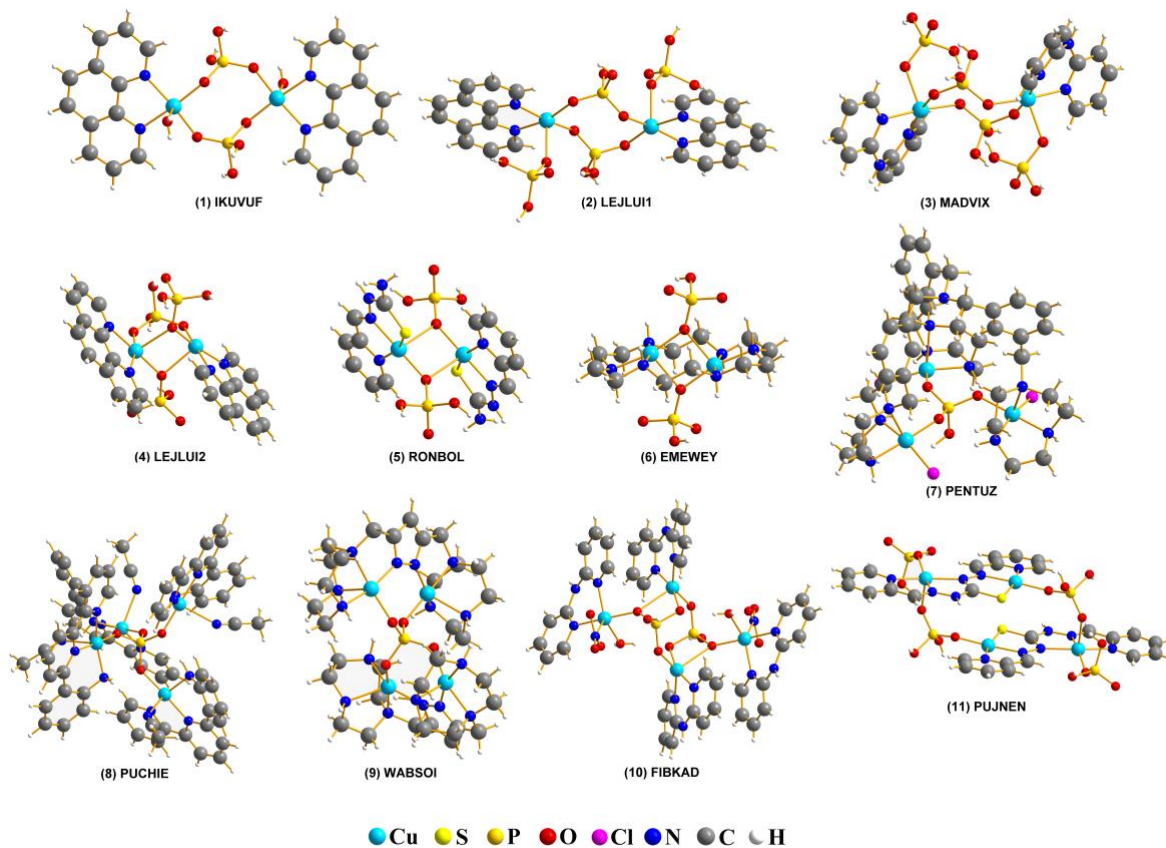


Figure 1. REFCODES and structures of the eleven studied systems taken from the CCDC crystallographic database.

Hydrogen positions were optimized using the BP86 functional, which has been previously proven to be better than the hybrid B3LYP, in conjunction with the Def2-TZVP basis set.³¹ In some cases, disordered positions of heavier atoms were encountered, and constrained optimizations for these centers were performed. It is worth noting that no paramagnetic ions, directly bonded to the donor atoms or bridging centers which mediate the superexchange interaction, were optimized in any case. Magnetostructural models for the 1,1- and 1,3- coordination modes of the phosphate anion were built following a similar procedure: (i) a central $\text{Cu}_2\text{H}_2\text{PO}_4$ moiety was constructed with typical distances for the phosphate ion and the O-Cu bond distance, (ii) the coordination environment of the Cu centers was completed with three ammonia ligands, completing a square planar

coordination (i.e. the three Cu-ammonia and the Cu-OPO₃ bonds are in the same plane and form right angles between them), (iii) bond distances, but not angles, were allowed to relax, (iv) hydrogen atoms were fully relaxed. After these steps, relevant bond angles were modified to scan the relevant geometric parameters for each model (*vide infra*) with no further optimization. For the 1,1-phosphate coordination mode, two models were built, one symmetric (two equal Cu-O distances) and one asymmetric. The later was considered based on a search on the CSD showing that most experimental cases have different Cu-O distances. The used values are in the average of the experimental ones (Cu1-O = 2.037 Å and Cu2-O = 2.500 Å).

Magnetic coupling constants were calculated under the broken-symmetry approach, following the $\hat{H} = -JS_1 \cdot S_2$ Hamiltonian.³²⁻³⁴ The non-projected formula for the relation of the coupling constant and the energies of the high spin and broken symmetry solutions were employed.³⁵ All calculations were carried out using the B3LYP density functional³⁶ and the Def2-TZVP basis set.³¹ Taking into account that coupling constants involve small energy differences (in the order of cm⁻¹), a larger integration grid (Grid7 in ORCA nomenclature) and very tight convergence criteria were employed in these calculations. In dinuclear Cu^{II} models, the only coupling constant can be directly obtained from the high spin (S=1) and the broken symmetry solution. In higher nuclearity complexes, it is possible to find several coupling constants, corresponding to the interaction of different pairs of paramagnetic centers. Several broken symmetry calculations are necessary to access exchange coupling constants of polynuclear systems. For a full description of the method see reference of Ruiz et al..³⁷ Considering that magnetic interactions occur between two paramagnetic centers, a substitution of all other paramagnetic centers, which do not belong to the evaluated exchange interaction, is done with Zn^{II} diamagnetic ions. Moreover, this substitution allows a clear visualization of the involved spin density in the evaluated exchange interaction. It is important to stress that the substitution does not affect the obtained *J* values.^{38,39} Diamagnetic substitution calculations were also employed to generate unrestricted corresponding orbitals (UCO), which resemble the notion of magnetic orbitals, as they maximize the one-to-one correspondence between doubly occupied orbitals, leaving the unpaired electrons in “magnetic”-like orbitals.⁴⁰

On the other hand, the canonical representation of orbitals produces that the unpaired electron density is being represented by several orbitals, thus making difficult to identify the magnetic orbital. For this reason most of the analyses have been done examining the empty beta orbital to identify the magnetic ones. Therefore the use of UCOs lowers the polarization effect obtained in the canonicals, thus giving the n unpaired electrons represented by n magnetic orbitals.

UCOs were further employed to generate and graphically represent the overlap function of the magnetic orbitals as the product of the unpaired electrons over a tridimensional grid. For clarity, the overlap functions obtained from the UCOs are plotted in light green and violet.

3. Results and discussion.

Based on the structural analysis of the studied structures (Table 1S), it becomes clear that there are many variables that can change simultaneously, such as bond distances, bond angles and phosphate coordination modes, as well as the number of bridges affecting the magnitude and nature of the different exchange interactions present in each studied structure. Due to the impossibility to find a clear and simple relation between the calculated J values with the nature of the phosphate bridges involved in the exchange pathways (metric values of each pathway listed in Table 1), a new parameter that will demonstrate the main factor that dominates the nature of the 1,3-PO₄ exchange pathway was proposed.

Table 1. Experimental and calculated exchange constants J (cm⁻¹) and coordination modes of the phosphate bridged copper compounds. The Cambridge Structural Database name (REFCODES), alongside with the corresponding number of copper centers of each compound is presented. Cu-Cu distances (Å), number and type of ligands of every exchange pathway, with the corresponding reference.

Compound	REFCODE	Number of Cu _{II} centers	d(Cu-Cu) (Å)	Phosphate-coordination	J_{calc} (cm ⁻¹)	J_{exp} (cm ⁻¹)	J label	Ref.
1	IKUVUF	2	5.0095(6)	1,3- H ₂ PO ₄ 1,3- H ₂ PO ₄	-14.9	-8.0	-	41
2	LEJLUI1	2	5.0430(1)	1,3- H ₂ PO ₄ 1,3- H ₂ PO ₄	-3.2	-8.2	-	42
3	MADVIX	2	5.1357(2)	1,3- H ₂ PO ₄ 1,3- H ₂ PO ₄	-3.5	-2.85	-	43
4	LEJLUI2	2	3.0742(5)	1,3- H ₂ PO ₄ 1,1- HPO ₄ ²⁻ 1,1- H ₂ PO ₄	-0.2	0.96	-	42
5	RONBOL	2	3.2950(2)	1,1- H ₂ PO ₄ 1,1- H ₂ PO ₄	0.6	AF	-	19
6	EMEWY	2	3.0362(8)	1,1- HPO ₄ ²⁻ 1,1- HPO ₄ ²⁻	-1.2	Not reported	-	44
7	PENTUZ	3	5.3916(5)	1,3- HPO ₄ ²⁻	4.0	Not reported	-	45
8	PUCHIE	4	5.2440(3) 5.2750(2)	1,3- PO ₄ ³⁻ 1,3- PO ₄ ³⁻	6.4; -0.7	Not reported	A B	46
9	WABSOI	4	5.6392(8) 5.3199(8) 5.7772(8) 4.8758(8) 4.0984(6) 4.0275(8)	1,3- PO ₄ ³⁻ 1,3- PO ₄ ³⁻ 1,3- PO ₄ ³⁻ 1,3- PO ₄ ³⁻ 1,3- PO ₄ ³⁻ -other* 1,3- PO ₄ ³⁻ -other*	-15.2 3.2 5.7 8.2 -47.4 -57.8	Not reported	A B C D	47
10	FIBKAD	4	4.8953(7) 4.1359(6) 4.5597(6)	1,3- H ₂ PO ₄ 1,3- H ₂ PO ₄ 1,1- H ₂ PO ₄ 1,3- H ₂ PO ₄ 1,3- H ₂ PO ₄	0.7 -27.5 -11.7	Not reported	i ii iii	48
11	PUJNEN	4	5.070(2) 4.983(2) 3.798(2)	1,3- H ₂ PO ₄ Not phosphate [†] Not phosphate [§]	-0.3 -97.3 -1.5	-105	A	20

* Pyrazole ; [†]pyridine-2-aldehyde thiosemicarbazone ; [§] bis(pyridine-2-aldehyde) thiocarbohydrazone

The relative Cu-phosphate and Cu-Cu orientations were measured considering how the Cu_{II} centers are positioned with respect to a dummy atom located on a vector projected from the phosphorus atom (P-D; D=dummy atom) and lying in the intersection between the two O-P-O planes of the phosphate bridge, thus defining two dihedral D-P-O_i-Cu_i (□) angle (Figure 2).

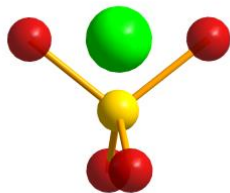


Figure 2. Model of a dummy atom located in an O-P-O plane. Red: oxygen atoms, yellow: phosphorus atom, green: dummy atom.

Based on this convention, two D-P-O-Cu dihedral angles were obtained for each Cu-phosphate-Cu exchange pathway in all the studied structures (Table 1S). This new parameter will give an idea about the relative orientation between the $d(x^2-y^2)$ magnetic orbitals of the interacting copper centers and their propagation and directionality through the phosphate bridges. Consequently, in order to evaluate how this parameter will influence the nature of the magnetic interaction between two interacting Cu^{II} centers, dinuclear models with 1,3-phosphate bridges were constructed and their different coupling constants were calculated.

For the more simple interaction given by a 1,1-PO₄ bridge, two models with Cu-O bond distances, symmetric and asymmetric, varying the Cu-O-Cu (θ) angle were constructed. The Cu-O distances obtained from a search of similar systems in the CSD showed both, symmetric and asymmetric bonds.

3.1. Magnetostructural 1,1- phosphate coordination model

Figure 3 shows the triprotonated 1,1-PO₄ asymmetric model of two triaminocopper(II) complexes in a square coordination geometry. Two different families were built, the first considering equal Cu-O distances (Cu1-O = Cu2-O = 2.037 Å), and a second family with different Cu-O distances (a distorted bridge with Cu1-O = 2.037 Å and Cu2-O = 2.500 Å). The Cu1-O-Cu2 angle θ is the variable parameter, varying from 135° to 90°. The calculated J values for both families as a function of the θ value are shown in Figure 4.

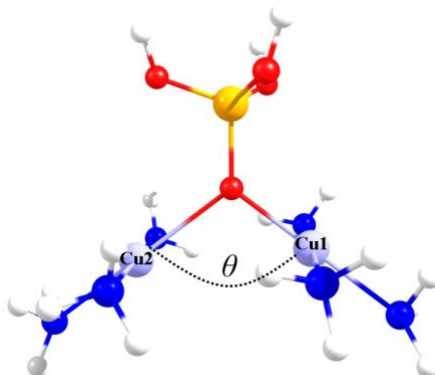


Figure 3. The triprotonated 1,1-PO₄ asymmetric model, defining θ as the Cu-O-Cu angle. Red: oxygen atoms, yellow: phosphorus atom, light blue: copper atoms, blue: nitrogen atoms, white: hydrogen atoms.

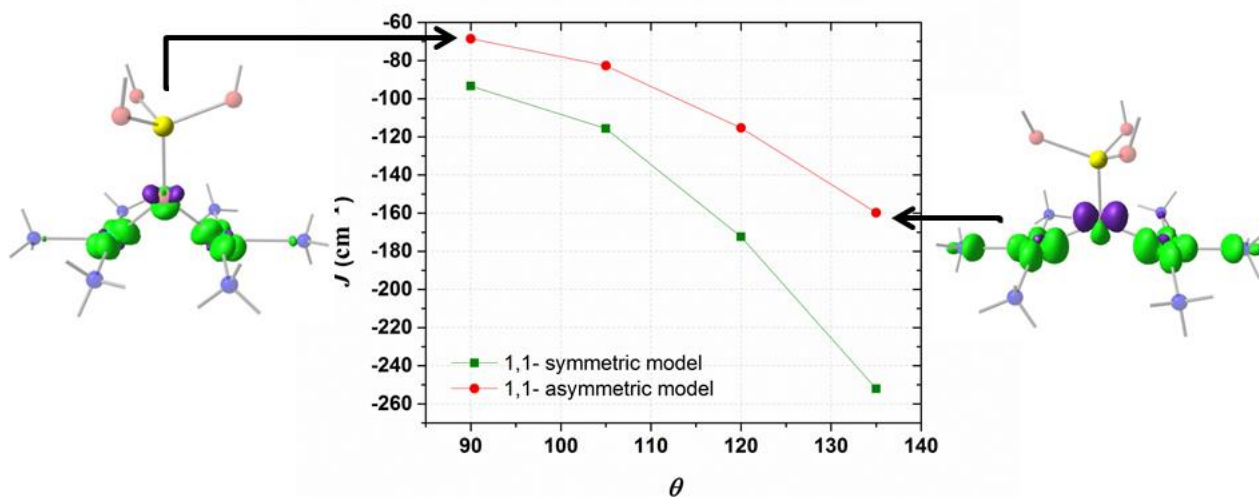


Figure 4. Obtained J values for the evaluated symmetric and asymmetric 1,1-PO₄ models. The overlap surfaces of the asymmetric model with $\theta = 90^\circ$ and $\theta = 135^\circ$ are shown. Light red: oxygen atoms, yellow: phosphorus atom, light blue: copper atoms, blue: nitrogen atoms. Overlap functions are plotted in green and violet. (Contour isovalue = 0.0012). Hydrogen atoms were omitted for clarity.

The model with asymmetric Cu-O bond distances has lesser antiferromagnetic behavior than the model with the symmetric ones, for all θ values (Figure 4). The overlap surfaces obtained from the UCOs of the model with the smallest studied angle ($\theta = 90^\circ$), showed that the size of the lobes of opposite phases on the oxygen atom are similar, thus not favoring the interaction (Figure 4, left). In the case the model with $\theta = 135^\circ$ the opposite lobes showed different sizes, favoring the antiferromagnetic interaction. In both 1,1- phosphate coordination models a larger angle produces a larger overlap that leads to a stronger antiferromagnetic coupling. Therefore the use of the calculated overlap surfaces generated from the UCOs is a good tool to predict the overlap both by the size and directionality of the lobes.

3.2. Magnetostructural 1,3-phosphate coordination model

The dinuclear magnetostructural 1,3-PO₄ model was built starting from the situation where both Cu-O vectors are collinear Figure 1Sa. The clock depicted in the upper left corner of the figure is the convention used for the values of the dihedral D-P-O-Cu (τ) angles (D the dummy atom), being in this particular case both dihedral angles equal to zero, with the Cu1-O1 and Cu2-O2 vectors collinear. In this situation both P-O1-Cu1 and P-O2-Cu2 angles are of 144.7° , value which was kept constant in the generation of all the studied models. Additionally, the eclipsed “trans-like” 1,3-model with D-P-O1-Cu1 = 90° and D-P-O2-Cu2 = 270° is shown in Figure 1Sb.

The rest of the 1,3-models were developed by scanning every 30° the dihedral τ , i.e. for a fixed value of D-P-O1-Cu1 = 30° , D-P-O2-Cu2 was scanned from 0° to 360° every 30° , and so on. This scanning produces two virtual cones in the structure as shown in Figure 2S. Due to this possibility to move around virtual cones, the nomenclature of *syn-syn*, *syn-anti* and *anti-anti* cannot be used as is done for planar ligands, such as carbonate and carboxylates. However, three points can be correlated with this nomenclature, being $(0^\circ, 0^\circ)$ *anti-anti*, $(0^\circ, 180^\circ)$ *syn-anti* and $(180^\circ, 180^\circ)$ *syn-syn*.

It is important to stress that in the depicted models both triamino-copper planes are coplanar. Calculations varying the coplanarity in the range of 0° to 90° showed no influence on the obtained J values. This is an expected result, due to the fact that this

rotation has a σ -type symmetry of the interaction of the magnetic orbital of the copper centers with the phosphate bridge.

In order to avoid any ambiguity in the definition of the dihedral D-P-O_i-Cu_i (τ) angles and the relative orientation, the following convention was defined:

1. For an equal value of both dihedral angles, both O_i-Cu_i vectors are parallel and eclipsed
2. For the antiparallel or “trans-like” orientation of the O-Cu bonds, the angle between both vectors is 180°. (Figure 1Sb)

In this way due to the symmetry around 180°, any point will have four symmetric equivalent points in a 360°/360° graph. For example, the (30°, 60°) configuration is equivalent to (60°, 30°) and (300°, 330°) and (330°, 300°). Conveniently this approach allows an unequivocal assignment of the position of a particular configuration, regardless of any sign convention in the measurement of the dihedral angles.

The 2D diagram depicted in Figure 5 shows the magnetic behavior obtained for the different rotation τ angles evaluated in the 1,3-model; the pink color represents the ferromagnetic cases and the blue color the antiferromagnetic ones. It is important to remark that the graph was generated with an antiferromagnetic scale from 0 to -80 cm⁻¹, while the ferromagnetic one from 0 to +10 cm⁻¹. The decrease of the intensity of both colors was used to show the gradual change between the ferro- and the antiferromagnetic behavior, i.e., where the magnetic interactions are very weak. The axes in the diagram are referred to the rotation of both D-P-O_i-Cu_i angles of the model. The 1,3-model shown in Figure 5 where both Cu-O vectors are collinear ($\square = 0^\circ$ for both copper centers), corresponds to the origin of the diagram (0°, 0°) being the most antiferromagnetic evaluated case. The magnetic behavior through the diagonal from (0°, 0°) to (360°, 360°) in which both angles vary in the same value and the same direction, is always antiferromagnetic, decreasing its value in the range of (130°, 130°) to (270°, 270°). On the other hand, the magnetic behavior for different angles and different orientations, i.e. the other diagonal from (0°, 360°) to (360°, 0°) changes from antiferro- to ferromagnetic.

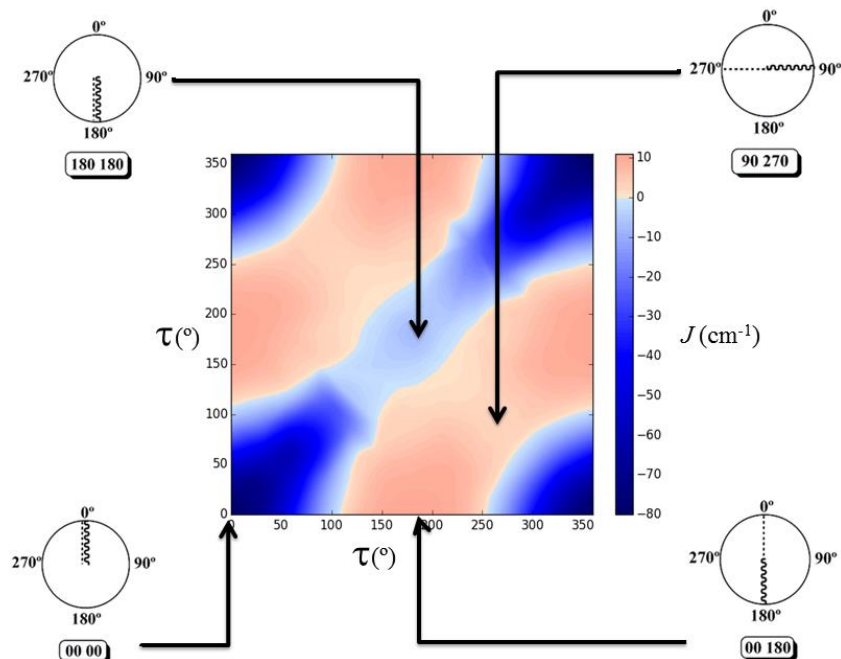


Figure 5. 2D diagram of the magnetic behavior obtained for the different rotation of the D-P-O_i-Cu_i (\square) angles for the 1,3-model. Selected combinations of dihedral angles for the 1,3-model using the clock representation are shown in the figure. Color code of the magnetic interaction (J in cm^{-1}) at the right side of the diagram (blue for antiferromagnetic and pink for ferromagnetic interaction).

Using Figure 6, four different cases will be discussed, a strong antiferromagnetic ($0^\circ, 0^\circ$) and a weak one ($180^\circ, 180^\circ$); a strong ferromagnetic ($0^\circ, 180^\circ$) and a weak one ($90^\circ, 270^\circ$). For the antiferromagnetic cases, the calculated overlap surfaces from the UCOS of the ($0^\circ, 0^\circ$) model showed that this has the largest surface size and favorable signs and directionality for the interaction between the copper and the oxygen atoms, thus being the most antiferromagnetically coupled model. The ($180^\circ, 180^\circ$) which is also antiferromagnetically coupled but in a less extent, the overlap surfaces show that the directionality of the lobes on the oxygen atoms and the copper atoms only permit a smaller overlap with respect to the ($0^\circ, 0^\circ$) model (Figure 6). On the other hand, the less ferromagnetic system ($90^\circ, 270^\circ$) shows an unfavorable overlap between the lobes of different signs between the copper centers and the oxygen atoms. The most ferromagnetic

system (0° , 180°) lacks of overlap surface on one of the oxygen atoms thus increasing the ferromagnetism, Figure 6.

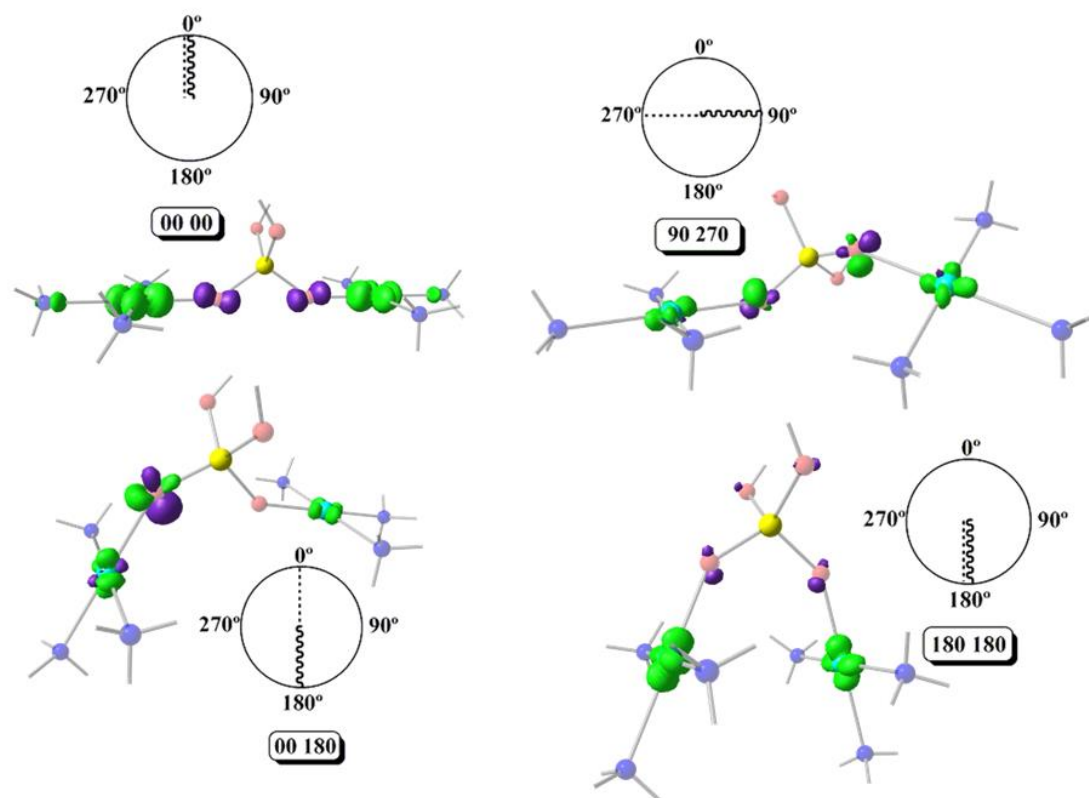


Figure 6. The overlap surfaces obtained for the 1,3-model with (0° , 0°); (90° , 270°); (0° , 180°) and (180° , 180°). Overlap functions are plotted in light green and violet. (Contour isovalue= 0.0012). Light red: oxygen atoms, yellow: phosphorus atom, light blue: copper atoms, blue: nitrogen atoms. Hydrogen atoms were omitted for clarity.

In order to test the proposed models eleven polymetallic molecular structures were selected from the CSD database, and their magnetic coupling constants were calculated with DFT methods (Table 1 and Table 1S). Table 1 summarizes the calculated magnetic coupling constants, J , for the eleven studied structures along with the reported experimental values (in the cases where the magnetic study was reported). The obtained J values span from antiferromagnetic to ferromagnetic. Selected structural parameters related with the

exchange pathways and the corresponding calculated J values for each structure are shown in Table 1.

Structures **1** to **6** are dinuclear compounds with two (**1**, **2**, **3**, and **6**) and three (**4** and **5**) protonated phosphate groups as bridges between the Cu^{II} centers. Structure **7** is a trinuclear one with one central $\{\text{HPO}_4\}$ group connecting the three copper centers, while the other four structures (**8** to **11**) have four Cu^{II} centers connected through one central $\{\text{PO}_4\}$ group. Except for **10** and **11**, the Cu^{II} atoms are five-coordinated within the studied structures. In **10** two of the four Cu^{II} centers are six-coordinated and the other ones are five-coordinated, while two of the Cu^{II} centers in **11** are four-coordinated and the other two five-coordinated.

The pure 1,3-phosphate connectivity mode for the Cu^{II} centers is found in structures **1**, **2**, **3**, **7**, **8**, **9**, and **11**, while the pure 1,1-phosphate connectivity mode is found in **5** and **6**. Structures **4** and **10** present mixed 1,1- and 1,3-coordination modes of the phosphate groups.

As can be observed in Table 1 the Cu–Cu distances vary from 3.036 Å to 5.777 Å, being the shortest distances those that include at least one 1,1- PO_4 as a bridge. The Cu–O–Cu angles of the structures with 1,1- PO_4 bridges have values ranging from 92.8° to 97.2°. The Cu–O–P angles measured for the 1,3-phosphate bridged complexes have values in the range of 121.0° to 135.6°, while the values of the dihedral angles Cu–O–O–Cu are in the range of -143.8° to 168.8° (Table 1S). The latter angles represent the relative collinearity between the interacting Cu^{II} centers through the 1,3-phosphate bridge. In structure **10** a Cu–O–Cu angle of 137.7° is found, due to the presence of one phosphate group bridging simultaneously two copper centers in both modes 1,1- and 1,3- modes (Figure 7).

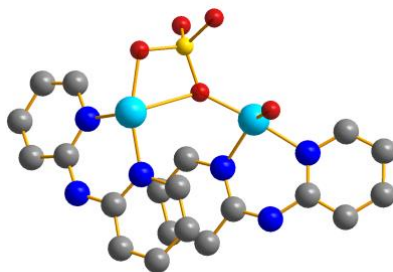


Figure 7. Simplified view of **10**, where a phosphate group is bridging two Cu^{II} centers in a 1,1- and 1,3- coordination mode simultaneously. Red: oxygen, yellow: phosphorus, light blue: copper, blue: nitrogen and grey: carbon atoms. Hydrogen atoms were omitted for clarity.

Compound **7** has three equivalent Cu-Cu distances, therefore only one exchange pathway can be considered. Compounds **8** and **9** with six possible exchange pathways, only two different Cu-Cu distances are present in **8**, thus two J values are considered. While in the case of **9** the six Cu-Cu distances are different, thus six J values were calculated. Compounds **10** and **11**, both tetranuclear, have only five possible exchange pathways. However in both compounds only three different Cu-Cu distances can be found, therefore three J values are considered in each case.

Exchange interactions with pure phosphate bridges in 1,3- and 1,1- coordination modes, or both simultaneously not including other auxiliary ligand, showed from antiferro- to ferromagnetic values ranging from -27.5 to $+8.2$ cm⁻¹. On the other hand when a nitrogen-based auxiliary bridge together with a 1,3-phosphate are the exchange pathways, an increase of antiferromagnetism is produced with calculated J values of -47.4 , -57.8 and -97.3 cm⁻¹ for both bridges in **9** and one bridge in **11** respectively.

It is well known that the overlap of the magnetic orbitals is the key for the observed magnetic behavior. The overlap values (S_2) of the eleven studied structures and its correlation with the calculated J values were evaluated under the Kahn-Briat model.^{49,50} Figure 8 shows that this correlation follows, as expected, a linear tendency for the negative J values corresponding the highest overlap values with the most antiferromagnetic J constants. No linear correlation following the Kahn-Briat model could be expected for the values close to zero. In order to achieve a better understanding of the above-mentioned correlation, the surface of the overlap functions obtained from the UCOs of two representative ferromagnetic ($J = +6.4$ cm⁻¹ for **8**) and antiferromagnetic ($J = -15.2$ cm⁻¹ for **9**) cases are depicted in Figure 8. In both systems the representation is in agreement with the calculated J values, i.e. a more antiferromagnetic J value is due to a stronger overlap between the magnetic centers, producing a bigger overlap surface. The ferromagnetic

interaction for **8** PUCHIE-A (left) has smaller overlap surface and unfavorable orientation of the lobes, than the antiferromagnetic interaction for **9** WABSOI-A (right).

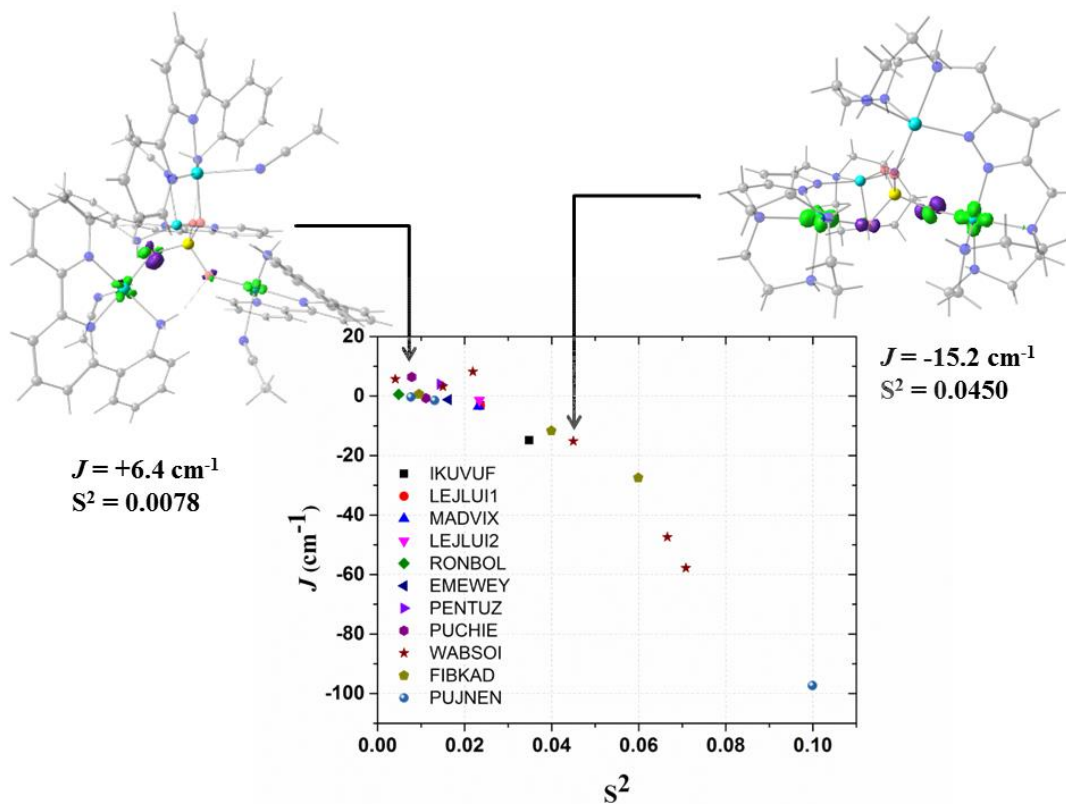


Figure 8. Plot of the calculated overlap (S^2) as a function of the calculated J values for compounds in Table 1, following the Kahn-Briat model. (PUCHIE-A (left): $J = +6.4 \text{ cm}^{-1}$; WABSOI-A (right), $J = -15.2 \text{ cm}^{-1}$). The overlap surfaces are plotted in light green and violet using a contour isovalue of 0.0012. Light red: oxygen atoms, yellow: phosphorus atom, light blue: copper atoms, blue: nitrogen, grey: carbon atoms. Hydrogen atoms were omitted for clarity.

In Figure 9 compound **11** (PUJNEN) which has three different magnetic pathways, the one with only an auxiliary N,N-based ligand shows the most antiferromagnetic calculated J value of -97.3 cm^{-1} . This is due to the favorable overlap between the $d(x^2-y^2)$ magnetic orbitals through the N,N-based ligand.

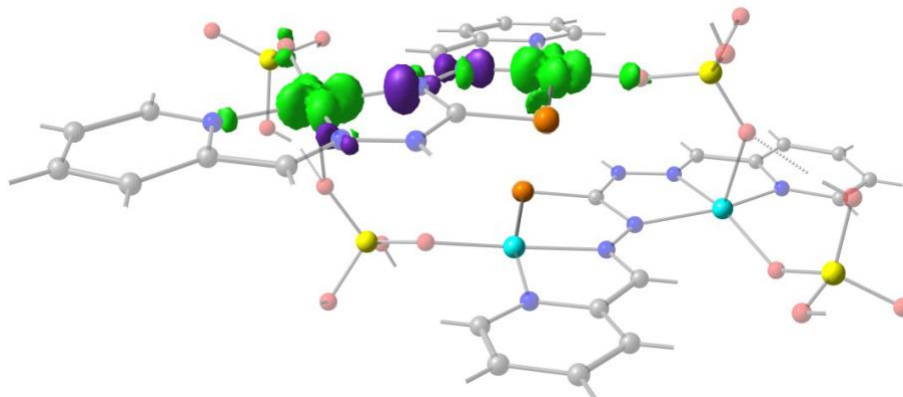


Figure 9. Overlap surfaces obtained from the UCOs for two representative Cu centers of compound **11** (PUJNEN) showing the predominant exchange through the N,N-ligand. (Contour isovalue of 0.0012). The overlap surfaces are plotted in light green and violet. Light red: oxygen, yellow: phosphorus, orange: sulfur, light blue: copper, blue: nitrogen and grey: carbon atoms. Hydrogen atoms were omitted for clarity.

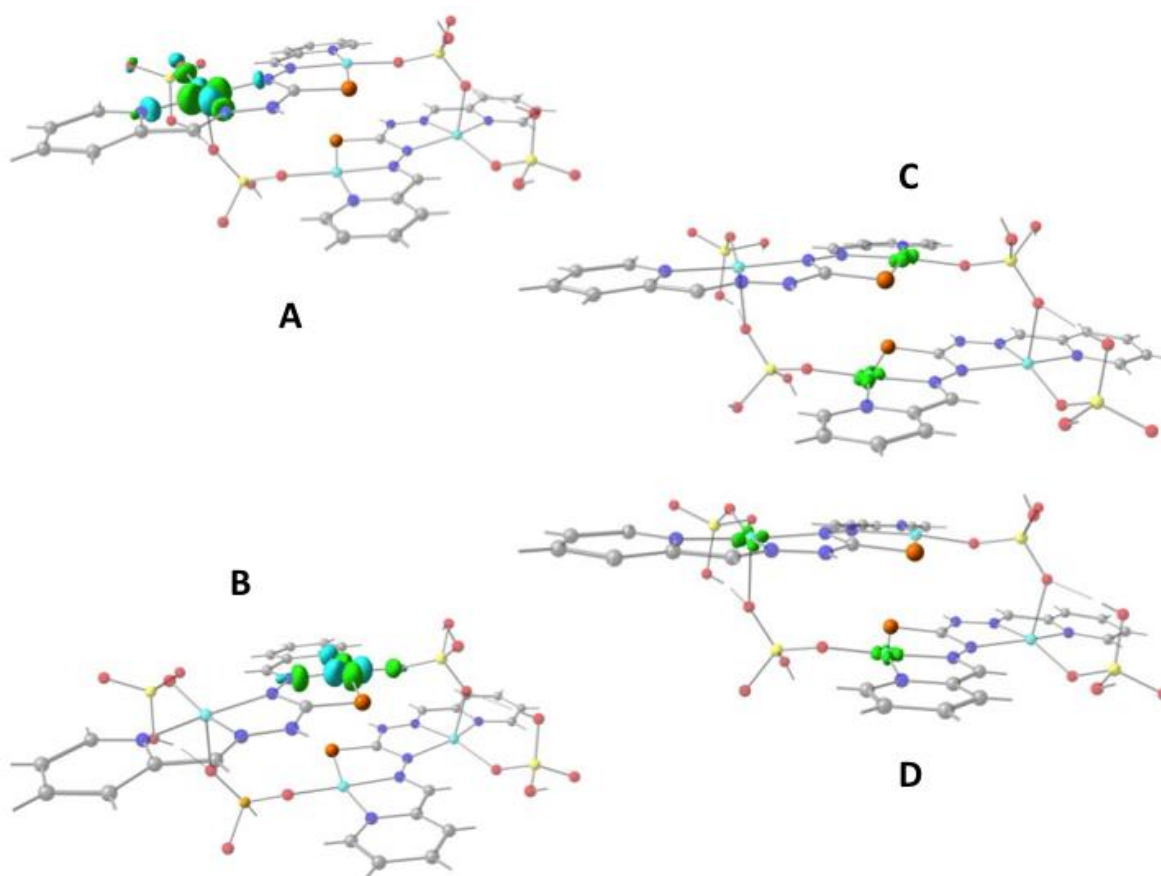


Figure 10. Unrestricted Corresponding Orbitals (UCO) for two representative Cu centers of compound **11**, (PUJNEN) (**A**, **B**); both signs of the surfaces are plotted in light green and light blue respectively using a contour isovalue = 0.10. Overlap surface for the sulfur exchange pathway (**C**), and phosphate pathway (**D**) both with contour isovalue = 0.0012. Light red: oxygen, yellow: phosphorus, orange: sulfur, light blue: copper, blue: nitrogen and grey: carbon atoms. Hydrogen atoms were omitted for clarity.

Figures 10A, 10B show that the magnetic orbitals $d(x^2-y^2)$ are positioned on the base of the square pyramid of each Cu^{II} center in the same plane of the nitrogen based ligand, thus leading to a large overlap. The second interaction in **11** including two sulfur bridges gives a calculated J value of -1.5 cm⁻¹. This low value is due to a very weak Cu-S-Cu' interaction, Cu-S ($d = 2.263$ Å) and Cu'-S ($d = 3.241$ Å), Figure 10C. It is clear that using the same contour isovalue as in the rest of the figures, a very small size of the lobes is obtained, reflecting the small exchange interaction through the sulfur. The third one which has only a 1,3-phosphate bridge (PUJNEN A), has also a small size of the lobes which is reflected in the calculated J value of -0.3 cm⁻¹, Figure 10D. However, this interaction of the phosphate bridge is equatorial to one copper center (in the same plane of the magnetic orbital) and axial to the second (perpendicular to the magnetic orbital). Therefore this interaction should not be included in the proposed model. Thus, the possibility of evaluating three different magnetic pathways gives a more precise interpretation of the magnetic phenomena of the tetranuclear species (PUJNEN). This gives an advantage in identifying the dominant magnetic pathways as compared to the analysis done by Mobaraki et al.²⁰ These authors used a simple dinuclear model, the Bleaney-Bowers expression, corrected by the Weiss constant, Θ , as the interdimer interaction to describe the tetranuclear complex.

Structure **9**, which has six different exchange pathways, two including an auxiliary N-N-pyrazole-based ligand together with a 1,3-phosphate bridge gave calculated J values of -47.4 and -57.8 cm⁻¹. As can be seen in Figure 11, the overlap between the Cu^{II} centers and the pyrazol ligand has the largest size of the surface and a favorable directionality of the lobes of different signs, contrary to that of the phosphate bridge; therefore the pyrazol produces a large overlap, thus favoring the antiferromagnetic behavior. On the other hand,

for the 1,3-phosphate, showing a poor overlap, it can be observed in Table 1S and Figure 12 that the values of the D-P-O-Cu angles indicate that this interaction should be weak ferromagnetic. The counter-complementarity of the orbitals will produce a predominant antiferromagnetic behavior as shown by the calculated J values (Table 1). It is important to stress that the use of the overlap surfaces, generated from the UCOs allowed identifying the predominant exchange pathway in this bi-bridged moiety. The central phosphate bridge produces four different pure 1,3- phosphate exchange interactions with three positive J values ($J = +3.2, +5.7$ and $+8.2$ cm⁻¹) and one negative one ($J = -15.2$ cm⁻¹).

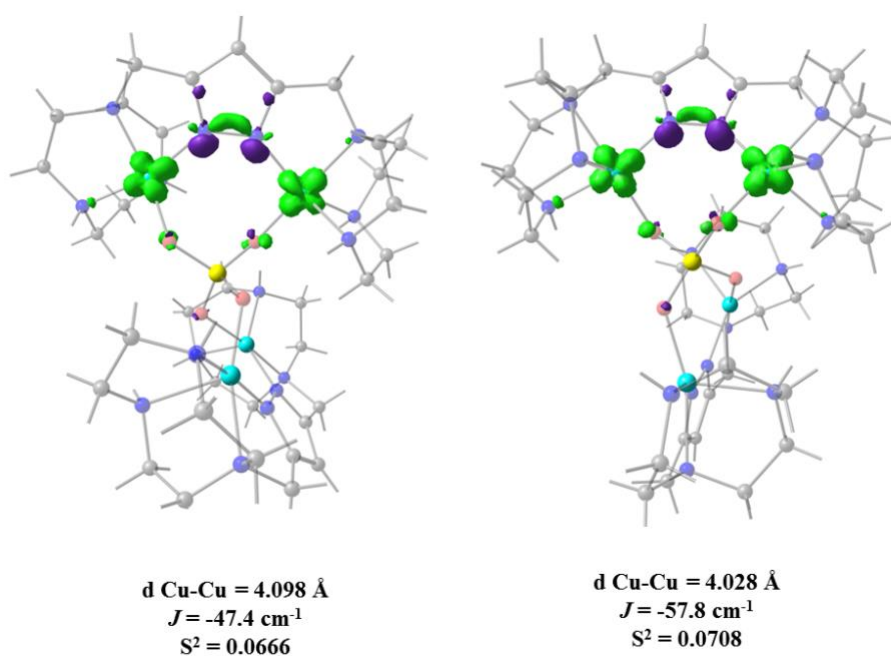


Figure 11. Overlap surfaces obtained from the UCOs, of the pathways that include auxiliary N-N-pyrazole ligands together with a 1,3-phosphate bridge in **9** (WABSOI) are plotted in light green and violet, using a contour value of 0.0012. Light red: oxygen, yellow: phosphorus, light blue: copper, blue: nitrogen and grey: carbon atoms. Hydrogen atoms were omitted for clarity.

One of the three calculated exchange constants of **10** with the highest antiferromagnetic character (Cu-Cu distance of 4.136 Å; $J = -27.5$ cm⁻¹) has pure-phosphate bridges in both 1,1- and 1,3- coordination mode simultaneously (Figure 7). This

structure contains four Cu^{II} centers interconnected through two {HPO₄} ligands, each one linking three centers simultaneously. In this interaction, the directionality of the magnetic orbitals allows a favorable overlap between the Cu^{II} centers through the 1,1-coordination mode of the phosphate unit (Cu-O-Cu angle of 137.7°), involving in a less extent the 1,3-coordination mode. The calculated overlap function permitted to demonstrate that the overlap in **10** was larger through the 1,1-phosphate bridge as compared to that of the 1,3-phosphate bridge, a fact that is impossible to infer from the experimental magnetization data.

In order to check the validity of the 2D correlation diagram with the magnetic data, all the exchange pathways through 1,3-phosphate were added to the diagram (Figure 12). As stated above the change in the color code of the ferromagnetic zone varies from weak ferromagnetic to a negligible magnetic interaction, thus the light pink color indicates a borderline interaction between ferro and antiferromagnetic interaction. As can be observed in the diagram PUCHIE-B (compound **8**) is in the central area of light pink color, being in the borderline situation.

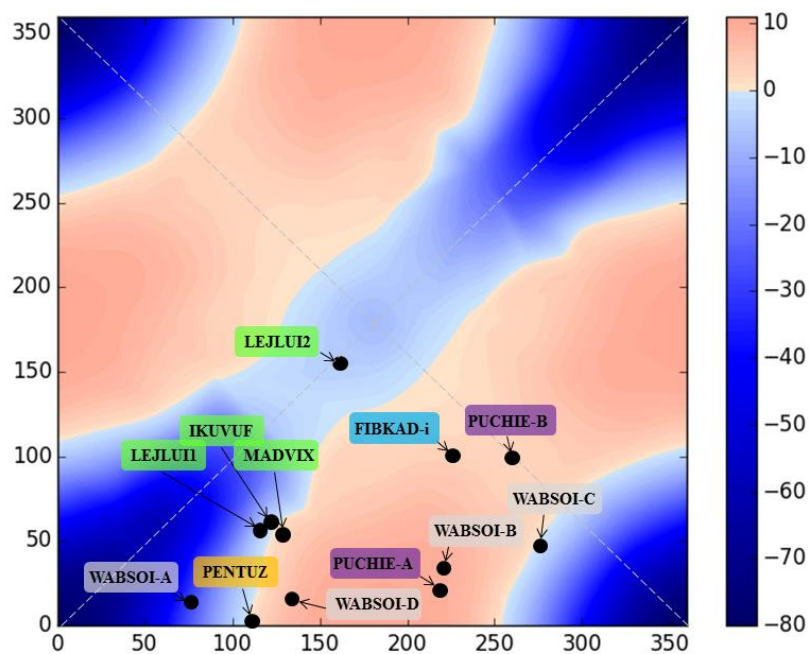


Figure 12. 2D correlation diagram for the 1,3-model, including the D-P-O_i-Cu_i angles of the pathways of structures **1**, **2**, **3**, **4**, **7**, **8**, **9**, **10** and **11**, that includes pure 1,3-phosphate bridges. The dotted lines show the four equivalent quadrants of the correlation.

All the compounds included in the analysis in Figure 12 have a magnetic pathway through 1,3-phosphate bridge. Compound **4** has a multiple bridge interaction with two 1,1-PO₄ and one 1,3-PO₄. Using the analysis of the overlap surfaces obtained from the UCOs (Figure 13), it becomes evident that only one 1,1-PO₄ and the 1,3-PO₄ bridges are participating in the exchange interaction. The Cu-O-Cu angle of the 1,1-PO₄ bridge is 92.8°, thus based on the results of the 1,1-model a weak antiferromagnetic interaction is expected. Moreover, the 1,1-PO₄ bridge is in the Jahn-Teller axis, thus the contribution to the overlap is negligible. On the other hand, the 1,3-PO₄, which is in the basal plane of the copper center, has the higher contribution to the magnetic exchange. The dihedral D-P-O_i-Cu_i angles of 155.3° and 161.4°, which according to the 1,3-model is in the weak antiferromagnetic zone. This result is in agreement with the calculated *J* constant (-0.2 cm⁻¹) (Figure 12).

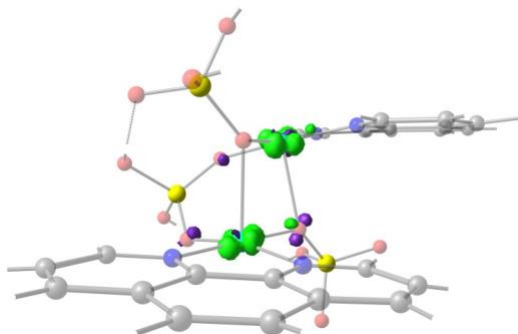


Figure 13. Overlap surface obtained from the UCOs for compound **4** (LEJLUI2), showing that the exchange pathway is through the 1,3 and the 1,1 bridges. Surfaces plotted in light green and violet, contour isovalue = 0.0012. Light red: oxygen, yellow: phosphorus, light blue: copper, blue: nitrogen and grey: carbon atoms. Hydrogen atoms were omitted for clarity.

Compound **10** has three different exchange pathways, FIBKAD-i (one 1,3-PO₄), FIBKAD-ii (one 1,3-PO₄ and one 1,1-PO₄) and FIBKAD-iii (two 1,3-PO₄). The first

pathway (FIBKAD-i) with a calculated ferromagnetic exchange ($J = +0.7 \text{ cm}^{-1}$) is in the 2D diagram in the ferromagnetic zone. For the second pathway, the surface analysis shows that both bridges are active in the transmission of the magnetic interaction, Figure 14. The 1,1- PO_4 has an Cu-O-Cu angle of 137.7° which produces a strong antiferromagnetic phenomenon (model 1,1; Figure 3). Moreover the 1,3- PO_4 bridge has dihedral angles of 183.9° and 19.9° , which correspond to a weak ferromagnetic interaction (less than $+10 \text{ cm}^{-1}$). Thus both simultaneous contributions corroborate the calculated $J = -27.5 \text{ cm}^{-1}$.

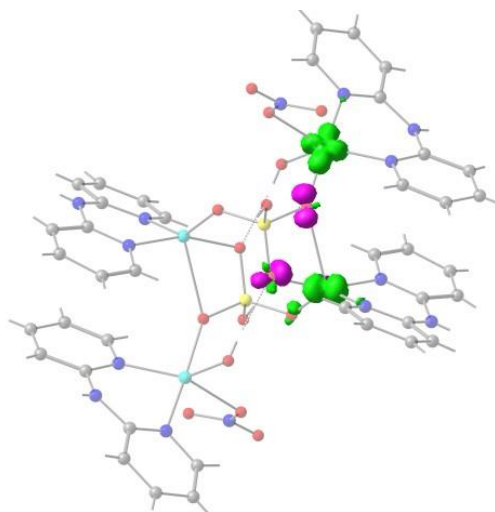


Figure 14. Overlap surface for compound **11** (FIBKAD-ii), showing that the exchange pathway is through both the 1,3 and the 1,1 bridges. Surfaces plotted in light green and violet, contour isovalue = 0.0012. Light red: oxygen, yellow: phosphorus, light blue: copper, blue: nitrogen and grey: carbon atoms. Hydrogen atoms were omitted for clarity.

The third exchange pathway has two 1,3- PO_4 bridges, the first with dihedral angles of 100.6° and 61.2° which produces a strong antiferromagnetism as can be deduced from Figure 11, while the second 1,3- PO_4 bridge has dihedral angles of 145.9° and 61.2° which corresponds to the limit of the antiferromagnetic zone (Figure 12). Therefore both interaction are in agreement with the calculated $J = -11.7 \text{ cm}^{-1}$.

In summary, using the magnetostructural 1,1- and 1,3- phosphate coordination models and the obtained overlap surfaces from the UCOs, it was possible to explain the calculated J values of all analyzed compounds.

4. Conclusions

For the symmetric and asymmetric 1,1-phosphate coordination models, a larger θ angle produces a larger overlap of the magnetic orbitals, leading to a stronger antiferromagnetic coupling. The symmetric model shows that the overlap interaction is more favorable than the obtained with the asymmetric one.

In the case of the 1,3-phosphate coordination mode the proposed model using the τ dihedral angle allows a systematic study of the magnetic behavior of experimental structures with phosphate bridges in this coordination mode.

In the case of the reported species that have pyrazole auxiliary ligands along with a 1,3-phosphate bridge, the overlap surfaces obtained from the UCOs permitted to infer that these auxiliary ligands are responsible for the main antiferromagnetic interaction, and that the phosphate groups have a much weaker role in the transmission of the magnetic phenomenon.

The used models have shown that antiferromagnetic exchange interactions is primarily produced by phosphate bridges, due to the plasticity of the bonding modes of the ligand that always enable a degree of overlap between the magnetic orbitals.

The relative orientation of the basal planes of each copper center is less relevant in the amount of exchange interaction, being the relative orientation of both Cu-O bonds the determining key factor.

Supporting Information.

The supporting information is available is available free of charge from the ACS publications website. Table 1S with structural parameters together with Figure 1S with schemes of different Cu-O relative angles and Figure 2S with the virtual cones formed by the scanning of the Cu-O angles.

Acknowledgements.

Authors acknowledge “Proyectos Basales and Vicerrectoría de Investigación, Desarrollo e Innovación” of Universidad de Santiago de Chile (USACH). Powered@NLHPC: This research was partially supported by the supercomputing infrastructure of the NLHPC (ECM-02). VPG, ES and DVY are members of CEDENNA Center (FB0807). E.R. thanks Ministerio de Economía y Competitividad for grant CTQ2015-64579-C3-1-P and Generalitat de Catalunya for an ICREA Academia grant.

Notes.

Dedicated to Professor Barry Lever on the occasion of his 80th birthday

References

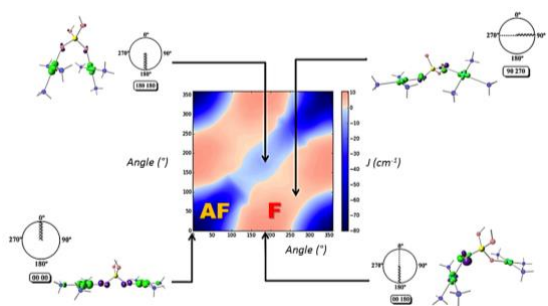
- (1) Su, K.; Jiang, F.; Qian, J.; Gai, Y.; Wu, M.; Bawaked, S. M.; Mokhtar, M.; AL-Thabaiti, S. A.; Hong, M. *Cryst. Growth Des.* **2014**, *14*, 3116–3123.
- (2) Ushak, S.; Spodine, E.; Venegas-Yazigi, D.; Fur, E. Le; Pivan, J. Y.; Peña, O.; Cardoso-Gil, R.; Kniep, R. *J. Mater. Chem.* **2005**, *15*, 4529.
- (3) Spodine, E.; Venegas-Yazigi, D.; Ushak, S.; Le Fur, E.; Pivan, J.-Y. *Phys. B Condens. Matter* **2006**, *384*, 120–122.
- (4) Ushak, S.; Spodine, E.; Venegas-Yazigi, D.; Le Fur, E.; Pivan, J. Y. *Microporous Mesoporous Mater.* **2006**, *94*, 50–55.
- (5) Ushak, S.; Spodine, E.; Le Fur, E.; Venegas-Yazigi, D.; Pivan, J.; Schnelle, W.; Cardoso-Gil, R.; Kniep, R. *Inorg. Chem.* **2006**, *45*, 5393–5398.
- (6) Spodine, E.; Venegas-Yazigi, D.; Ushak, S.; Paredes-García, V.; Saldias, M.; Le Fur, E.; Pivan, J. Y. *Polyhedron* **2007**, *26*, 2121–2125.
- (7) Venegas-Yazigi, D.; Muñoz-Becerra, K.; Spodine, E.; Brown, K.; Aliaga, C.; Paredes-García, V.; Aguirre, P.; Vega, A.; Cardoso-Gil, R.; Schnelle, W.; Kniep, R. *Polyhedron* **2010**, *29*, 2426–2434.
- (8) Lu, Y.; Wang, E.; Guo, Y.; Xu, X.; Xu, L. *J. Mol. Struct.* **2005**, *737*, 183–187.
- (9) Doyle, R. P.; Kruger, P. E.; Moubaraki, B.; Murray, K. S.; Nieuwenhuyzen, M. *Dalt. Trans.* **2003**, *2003*, 4230.
- (10) Jian, F.-F.; Tong, Y.-P.; Xiao, H.-L.; Sun, P.-P.; Zhao, P.-S. *Acta Crystallogr. Sect. C Cryst. Struct. Commun.* **2004**, *60*, m348–m349.
- (11) Liu, H.-X.; Jiang, X.; Liang, Y. *Acta Crystallogr. Sect. E Struct. Reports Online* **2007**, *63*, m1472–m1472.
- (12) Davenport, T. C.; Ahn, H. S.; Ziegler, M. S.; Tilley, T. D. *Chem. Commun.* **2014**, *50*, 6326.

- (13) Yan, J.; Zhao, X.; Huang, J.; Gong, K.; Han, Z.; Zhai, X. *J. Solid State Chem.* **2014**, *211*, 200–205.
- (14) Lambert, S. L.; Felthouse, T. R.; Hendrickson, D. N. *Inorganica Chim. Acta* **1978**, *29*, L223–L224.
- (15) Doyle, R. P.; Bauer, T.; Julve, M.; Lloret, F.; Cano, J.; Nieuwenhuyzen, M.; Kruger, P. E. *Dalton Trans.* **2007**, 5140–5147.
- (16) Allen, F. H. *Acta Crystallogr. Sect. B Struct. Sci.* **2002**, *58*, 380–388.
- (17) Zhu, H.-L.; Jin, L.; Cheng, D.-Y.; Zheng, Y.-Q. *Inorganica Chim. Acta* **2012**, *388*, 37–45.
- (18) Doyle, R. P.; Julve, M.; Lloret, F.; Nieuwenhuyzen, M.; Kruger, P. E. *Dalt. Trans.* **2006**, 2081.
- (19) Ainscough, E. W.; Brodie, A. M.; Ranford, J. D.; Waters, J. M. *J. Chem. Soc. Dalt. Trans.* **1997**, 1251–1256.
- (20) Moubaraki, B.; Murray, K. S.; Moubaraki, B.; Ranford, J. D.; Wang, X.; Xu, Y. *Chem. Commun.* **1998**, *8*, 353–354.
- (21) Spiccia, L.; Graham, B.; Hearn, M. T. W.; Lazarev, G.; Moubaraki, B.; Murray, K. S.; Tiekink, E. R. T. *J. Chem. Soc., Dalt. Trans.* **1997**, 4089–4097.
- (22) Crawford, V. H.; Richardson, H. W.; Wasson, J. R.; Hodgson, D. J.; Hatfield, W. E. *Inorg. Chem.* **1976**, *15*, 2107–2110.
- (23) Ruiz, E.; Alemany, P.; Alvarez, S.; Cano, J. *J. Am. Chem. Soc.* **1997**, *119*, 1297–1303.
- (24) Venegas-Yazigi, D.; Aravena, D.; Spodine, E.; Ruiz, E.; Alvarez, S. *Coord. Chem. Rev.* **2010**, *254*, 2086–2095.
- (25) Doyle, R. P.; Kruger, P. E.; Julve, M.; Lloret, F.; Nieuwenhuyzen, M. *CrystEngComm* **2002**, *4*, 13.

- (26) Amos, A. T.; Hall, G. G. *Proc. R. Soc. A Math. Phys. Eng. Sci.* **1961**, *263*, 483–493.
- (27) King, H. F. *J. Chem. Phys.* **1967**, *47*, 1936.
- (28) Aravena, D.; Ruiz, E. *Chem. - A Eur. J.* **2011**, *17*, 8841–8849.
- (29) Neese, F. *Wiley Interdiscip. Rev. Comput. Mol. Sci.* **2012**, *2*, 73.
- (30) An ab initio, DFT and semiempirical SCF-MO package-Version 3.0 Design and Scientific Directorship: F. Neese; Technical Directorship: F. Wennmohs, Max-Planck-Institute for Chemical Energy Conversion Stiftstr. 34-36, 45470 Mülheim a. d. Ruhr, Germany, tccec@mpi-mail.mpg.de. With contributions from: U. Becker, D. Bykov, D. Ganyushin, A. Hansen, R. Izsak, D.G. Liakos, C.Kollmar, S. Kossmann, D.A. Pantazis, T. Petrenko, C. Reimann, C. Riplinger, M.Roemelt, B. Sandhöfer, I. Schapiro, K. Sivalingam, B. Wezislá, and contributions from our collaborators: M. Kallay, S. Grimme, E. Valeev, G. Chan.
- (31) Weigend, F.; Ahlrichs, R. *Phys. Chem. Chem. Phys.* **2005**, *7*, 3297.
- (32) Noodleman, L. *J. Chem. Phys.* **1981**, *74*, 5737.
- (33) Ginsberg, a. P. *J. Am. Chem. Soc.* **1980**, *102*, 111–117.
- (34) Bencini, A.; Gatteschi, D. *J. Am. Chem. Soc.* **1986**, *108*, 5763–5771.
- (35) Ruiz, E.; Cano, J.; Alvarez, S.; Alemany, P. *J. Comput. Chem.* **1999**, *20*, 1391–1400.
- (36) Becke, A. D. A. *J. Chem. Phys.* **1993**, *98*, 5648.
- (37) Ruiz, E.; Rodríguez-Forteá, A.; Cano, J.; Alvarez, S.; Alemany, P. *J. Comput. Chem.* **2003**, *24*, 982–989.
- (38) Saldias, M.; Paredes-García, V.; Vega, A.; Cañon-Mancisidor, W.; Le Fur, E.; Venegas-Yazigi, D.; Spodine, E. *Polyhedron* **2012**, *41*, 120–126.
- (39) Cañon-Mancisidor, W.; Gómez-García, C. J.; Espallargas, G. M.; Vega, A.; Spodine, E.; Venegas-Yazigi, D.; Coronado, E. *Chem. Sci.* **2014**, *5*, 324.

- (40) Neese, F. *J. Phys. Chem. Solids* **2004**, *65*, 781–785.
- (41) Moreno, Y.; Vega, A.; Ushak, S.; Baggio, R.; Peña, O.; Le Fur, E.; Pivan, J.-Y.; Spodine, E. *J. Mater. Chem.* **2003**, *13*, 2381.
- (42) Phuengphai, P.; Youngme, S.; Pakawatchai, C.; van Albada, G. A.; Quesada, M.; Reedijk, J. *Inorg. Chem. Commun.* **2006**, *9*, 147–151.
- (43) Youngme, S.; Phuengphai, P.; Chaichit, N.; Pakawatchai, C.; van Albada, G. a.; Roubeau, O.; Reedijk, J. *Inorganica Chim. Acta* **2004**, *357*, 3603–3612.
- (44) Barker, J. E.; Liu, Y.; Martin, N. D.; Ren, T. *J. Am. Chem. Soc.* **2003**, *125*, 13332–13333.
- (45) Cao, R.; Müller, P.; Lippard, S. J. *J. Am. Chem. Soc.* **2010**, *132*, 17366–17369.
- (46) Cargill Thompson, A. M. W.; Bardwell, D. A.; Jeffery, J. C.; Ward, M. D. *Inorganica Chim. Acta* **1998**, *267*, 239–247.
- (47) Raidt, M.; Neuburger, M.; Kaden, T. A. *Dalt. Trans.* **2003**, 1292–1298.
- (48) Youngme, S.; Phuengphai, P.; Chaichit, N.; van Albada, G. A.; Roubeau, O.; Reedijk, J. *Inorganica Chim. Acta* **2005**, *358*, 849–853.
- (49) Kahn, O.; Briat, B. *J. Chem. Soc. Faraday Trans. 2* **1976**, *72*, 268.
- (50) Kahn, O.; Briat, B. *J. Chem. Soc. Faraday Trans. 2* **1976**, *72*, 1441.

For Table of Contents



Models for the 1,1 and 1,3- bridging modes of phosphate for copper(II) compounds were developed in order to generate the angle dependence of J values. Using the unrestricted corresponding orbitals (UCO), a graphical assignment of the predominant exchange pathway was described.